Geometric Distortion in Structural Magnetic Resonance Imaging

Deming Wang* and David M. Doddrell

Centre for Magnetic Resonance, The University of Queensland, St. Lucia, QLD 4072, Australia

Abstract: Geometric distortion, an undesirable image artifact, is an inferior aspect associated with magnetic resonance imaging (MRI). Although slight distortions in MR images often have no consequences in reaching clinical conclusions, geometric distortions can make significant differences in certain MR applications such as, for example, stereotactic localization in radio-surgery and MR image-guided biopsy. In this article, geometric distortion in structural MRI is reviewed. It begins with a brief discussion of various sources that can cause geometric distortion in structural MRI, followed by a review of the apparatus and methods that have been developed for the measurement and characterization of the geometric distortion in MRI. The paper will then focus on a novel phantom-based technique that has been developed recently by the authors. This technique can provide a comprehensive and complete measurement of the geometric distortion in 3-dimensions with unprecedented details and accuracy. The major outcomes of a comprehensive study on the geometric distortion in representative clinical MR scanners, carried out recently using this technique, will be discussed. The article will also include a discussion of various correction methods that have been developed for correcting geometric distortion in MRI.

Keywords: Structural MRI, geometric distortion, gradient field nonlinearity, static field inhomogeneity, geometric phantom, correction.

1. INTRODUCTION

Geometric distortion has long been regarded as an inferior aspect of magnetic resonance imaging (MRI), an imaging modality that has revolutionized medical imaging in the past two decades. Although MRI has now become the preferred choice in many clinical examinations due to its superior capability to differentiate diseased tissues from healthy tissues and one tissue type from another, the possibility of geometric distortion being present in MR images still limits its full potential for use in some applications. One such application is image-guided radiosurgery [1-10]. In current practice, both MR and computerized tomography (CT) images are used in this technique. MRI is employed to provide better definition of a tumor, while CT is used for spatial localization in the treatment because of the possibility of the presence of geometric distortion in the MR images. This practice is not ideal as it is time consuming. Additionally, the co-registration procedure of aligning MR and CT images (often referred to as image fusion) can cause errors in spatial localization particularly if MR images contain significant geometric distortion. Another area of major concern related to geometric distortion is the MR image-based quantification. Obviously, any geometric distortion will ultimately lead to errors in the extracted volumes based on MR images.

Geometric distortion in MRI is a complex issue. Firstly, MRI is intrinsically a 3-dimensional (3D) volumetric imaging technique, therefore, geometric distortion in MRI needs to be understood in 3-dimensions. This is equally true in MR images acquired using the 2-dimensional (2D) imaging techniques. This point seems to have been overlooked in the past. Secondly, geometric distortion in MRI can arise from a variety of sources. Generally speaking, these sources can be classified as hardware-related and tissue-related. The main sources contributing to geometric distortion from MRI hardware are the inhomogeneity in the main magnet, the nonlinearity in the gradient fields and the eddy currents associated with the switching of the gradient coils. The tissue-related sources mainly include susceptibility difference and chemical shift. While the hardware-related sources can be measured and characterized for individual systems, tissue-related distortion is imaging object-dependent and its assessment normally requires special modeling. Thirdly, one of the unique features of MRI is its diversity. MRI is in fact a collection of many sequences (or techniques) that explore and manipulate a wide range of spin physical properties. As a result, the geometric distortion can be manifested quite differently in different sequences. For example, the geometric distortion due to the inhomogeneity in the main magnet and the susceptibility difference is very different in MR images acquired using a simple spin echo sequence from that obtained, for example, using echo planar imaging (EPI).

Due to the complexity of the issue, it is not our intention to attempt to cover all aspects of geometric distortion in MRI in this mini-review. It is, however, a fact that geometric distortion has been one of the intensively researched topics in MRI over the past two decades. Currently, there is extensive literature to be found on various aspects of geometric distortion in MRI. For example, the field inhomogeneity-related geometric distortion in MR images using fast imaging sequences such as EPI has received a great deal of interest [11-14]. The tissue susceptibility difference-related geometric distortion has also been studied widely [15-20]. This mini-review is mainly devoted to the geometric distortion in structural MRI principally caused by the inhomogeneity of the static field and the nonlinearity of

*Address correspondence to this author at the Centre for Magnetic Resonance, The University of Queensland, St. Lucia, QLD 4072, Australia; Tel: +61-7-33654100; Fax: +61-7-33653833; E-mail: deming@cmr.uq.edu.au

1573-4056/05 $50.00+.00

the gradient fields. Geometric distortion in structural MRI is an important issue, especially in neuroimaging. This review was written with a particular focus on two important application areas: MR image-based volumetric measurement and MR-image-based spatial localization.

Over the past decade, we have witnessed an explosion of publications on the use of structural MRI in the study of a wide range of brain diseases. Numerous publications have now appeared in the literature reporting the cross-sectional as well as longitudinal MRI studies on Alzheimer's disease, multiple sclerosis, epilepsy, and a range of other brain diseases. The primary information sought from the MR images in these studies is the structural information, mainly volumes and shapes. While findings from different groups seem to agree generally, discrepancies do exist. Some of these discrepancies were thought to be due to the heterogeneous nature of the disease or the errors (both subjective and objective in nature) associated with the derivation of the volumes from structural MRI. However, a potential source of errors that has been rarely investigated is the geometric distortion. The reason for this is probably due to the lack of an effective technique that can provide a convenient and accurate measurement of the geometric distortion in structural MRI, rather than ignorance. The lack of investigation on possible errors due to geometric distortion is particularly disturbing for longitudinal studies, as some of these studies have lasted for many years. The instability and possible upgrades of a scanner occurring during the study interval cannot guarantee the same performance in a given MR system for the entire study period.

As stated earlier, the possibility of geometric distortions in MRI limits its full potential in the application of image-guided radiation treatment. This is particularly the case in radiosurgery in which spatial localization of tumors in the brain is generally required within an accuracy of better than 1 *mm*. Although MRI scanners have been designed to have the most homogeneous static field and the linearity of the gradient fields around the isocentre, geometric distortion that falls within 1 *mm* inside a volume of the size of the human head (~180 *mm* in diameter) is still beyond the reach of most clinical MR scanners. Therefore, there has been a great deal of interest in the study of geometric distortions in MRI scanners [21-45], with a particular focus on the potential use for spatial localization in the treatment of brain tumors. However, most of these studies were carried out in 2D. In other words, geometric distortion was only investigated within the imaging plane and the distortion along the normal of the imaging plane was usually ignored. These incomplete measurements can be detrimental if the results are not cautiously used for treatment planning. MRI-guided treatment is also being considered in treating tumors in peripherial areas. Geometric distortion in MR systems can be significantly larger in areas further away from the isocentre.

This mini-review is organized as follows. In section 2, a brief description of the geometric distortion due to the inhomogeneity of the static field and the nonlinearity of the gradient fields is given. This is followed by a review of the methods that have been developed and used for the measurement and characterization of the geometric distortion in MRI (section 3). Hardware-related geometric distortion in MRI scanners currently in clinical service is reviewed in section 4. These include the systems with superconducting, resistive or permanent magnets. Methods developed for correcting geometric distortion in MRI are reviewed in section 5 and the final section (section 6) is devoted to some discussion.

2. MR HARDWARE-RELATED GEOMETRIC DISTORTION

Magnetic resonance Fourier imaging works on the simple principle of the conventional Fourier transform that relates the spatially encoded time-domain data to the frequency-domain data, namely the MR image. The underlying requirement is the use of spatially varying linear gradients that are used for the encoding of spatial information. Thus, any deviations from the linear behavior in the gradient systems (often referred to as gradient field nonlinearity) will cause geometric distortions in the resulting MR images. Of course, in this linear relationship, the main magnet that is used for polarizing the spins (the source of the MR signal) also needs to be uniform within the imaging volume. Any inhomogeneity in the main magnet (the static field) will cause geometric distortion in the presence of a gradient field.

The inhomogeneity in the static field is usually measured by the maximum deviation from a designed field strength (B_0) within a defined volume of interest.

$$\frac{\left| \max(B_z(x,y,z)) - B_0 \right|}{B_0}$$

The inhomogeneity is usually measured in units of ppm for a spherical volume. For superconducting magnets equipped with advanced shimming technologies, a uniformity of 1 ppm can be easily achieved. At 1.5 *T*, this translates to a maximum field deviation of 1.5 μT (micro Tesla). The corresponding geometric distortion in the presence of the gradients normally used in contemporary MRI systems (~2 *mT*/m or 2μT/mm) would be less than 1 *mm*. In low field systems with permanent or resistive magnets, the uniformity of the static field can be worse and it can lead to larger geometric distortions. Clearly, the magnitude of the geometric distortion due to the static field inhomogeneity is dependent on the gradient strength used. For example, at 1.5 *T* with a gradient of 1.5 *mT*/*m*, each part per million of inhomogeneity would result in a distortion of 1 *mm*. This distortion is halved if a gradient of 3 *mT*/*m* is used. In additio n, th e static field inhomogeneity mainly causes geometric distortion along the readout (frequency-encoding) direction and slice selection direction (in 2D techniques) but not along the phase encoding direction as phase encoding is insensitive to field inhomogeneity [44].

The spatial characteristics of the gradient fields generated by a MR gradient sub-system can be compactly described by the so-called gradient coil tensor, $\boldsymbol{L}(\boldsymbol{r})$ [46]. This tensor is defined as

$$\begin{pmatrix} G_x^{act}(\boldsymbol{r}) \\ G_y^{act}(\boldsymbol{r}) \\ G_z^{act}(\boldsymbol{r}) \end{pmatrix} = \begin{pmatrix} L_{xx}(\boldsymbol{r}) & L_{xy}(\boldsymbol{r}) & L_{xz}(\boldsymbol{r}) \\ L_{yx}(\boldsymbol{r}) & L_{yy}(\boldsymbol{r}) & L_{yz}(\boldsymbol{r}) \\ L_{zx}(\boldsymbol{r}) & L_{zy}(\boldsymbol{r}) & L_{zz}(\boldsymbol{r}) \end{pmatrix} \begin{pmatrix} G_x \\ G_y \\ G_z \end{pmatrix}$$

where $\boldsymbol{G_i^{act}}$ ($i = x, y$ and z) are the components of the actual gradient generated by the gradient coils (X, Y and Z) and G_x, G_y and G_z are the designed nominal gradient strengths. If the gradients are perfectly linear, the gradient coil tensor is reduced to the 3×3 identity matrix, $\boldsymbol{I}$. Thus, the gradient coil tensor $\boldsymbol{L}(\boldsymbol{r})$ can be decomposed into a linear part ($\boldsymbol{I}$) and a nonlinear part denoted as $\tilde{L}(\boldsymbol{r})$

$$\boldsymbol{L}(\boldsymbol{r}) = \boldsymbol{I} + \tilde{\boldsymbol{L}}(\boldsymbol{r})$$

where

$$\boldsymbol{I} = \begin{pmatrix} 1 & 0 & 0 \\ 0 & 1 & 0 \\ 0 & 0 & 1 \end{pmatrix}$$

and

$$\tilde{\boldsymbol{L}}(\boldsymbol{r}) = \begin{pmatrix} L_{xx}(\boldsymbol{r}) - 1 & L_{xy}(\boldsymbol{r}) & L_{xz}(\boldsymbol{r}) \\ L_{yx}(\boldsymbol{r}) & L_{yy}(\boldsymbol{r}) - 1 & L_{yz}(\boldsymbol{r}) \\ L_{zx}(\boldsymbol{r}) & L_{zy}(\boldsymbol{r}) & L_{zz}(\boldsymbol{r}) - 1 \end{pmatrix}$$

clearly, $\tilde{\boldsymbol{L}}\ (\boldsymbol{r})$ provides a complete description of the gradient field non-linearity. It is this nonlinear part that can cause a range of undesirable effects including geometric distortion in MR images. In MRI systems with superconducting magnets, it is the gradient field nonlinearity that contributes most to the observed geometric distortion (more in section 4). This is particularly the case in the new generation of MR systems in which shorter gradient coils are used for producing fast-switching gradients.

The geometric distortion in MRI due to the static field inhomogeneity and the nonlinearity of the gradient fields is 3D in nature. This is true, both in the use of 2D (slice selection), and 3D (volumetric) imaging techniques. The 3D nature of the geometric distortion in MRI appears to have been overlooked in the past as most studies carried out on geometric distortion in MRI were in 2D. Let's use a simple example to illustrate the 3D nature of the geometric distortion in MRI. In Fig. **1**, the geometric distortion studied using a grid phantom is shown. Here, the geometric distortion is only measured in the slice plane (the imaging plane). The distortion along the normal of the plane in this 2D method is not measured. In fact, an assumed "flat" slice plane in 2D methods (schematically shown in Fig. **2a**) may look more like the one shown in Fig. **2b**, a curved surface, due to the distortion along the normal of the slice plane. Therefore, with any 2D methods, this information is unobtainable and the measurement is incomplete. A complete measurement of the geometric distortion in MRI clearly requires a 3D approach. This is schematically shown in Fig. **3** using a cube. Here, the known positions of the points on the surfaces of the cube in the undistorted space (represented as grid points in Fig. **3a**) are completely tracked down in 3D in the distorted image space (Fig. **3b**).

3. MEASUREMENT AND CHARACTERIZATION OF GEOMETRIC DISTORTION IN MRI

Geometric distortion in MRI has usually been measured and studied by specially designed geometric phantoms.

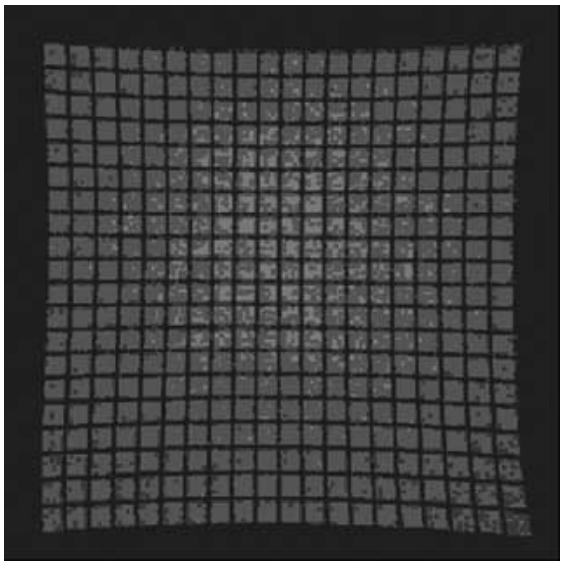

Fig. (1). A MR image from a 2D grid phantom showing the geometric distortion in the imaging plane.

There are a large number of geometric phantoms that have been specifically designed for the measurement of geometric distortion in MRI by various research groups [24,26,27,29,30,34,35,40,41,45]. In addition, MR vendors provide their customers with a set of phantoms which usually include one for geometric distortion for calibration and quality checks. Relevant professional societies have also developed special phantoms for their own acceptance tests and for regular monitoring of the performance of MRI systems in clinical service [47-51].

The basic idea used in the design of geometric phantoms for geometric distortion measurement in MRI is very simple. Geometric phantoms usually contain a set of reference points, or features that can be easily identified in MR images. For easy reference, these reference points or features will be called "control points" hereafter. By establishing the correspondence between the locations of the control points in the distorted MR image and their known positions defined by the geometry of the phantom, geometric distortion is then measured. Among some of the developed phantoms, the control points are only defined in 2-dimensions. These phantoms are thus referred to as 2D phantoms in order to distinguish them from those with the control points defined fully in 3D (therefore, referred to as 3D phantoms). In the following, a brief discussion is given on some of the 2D and 3D phantoms developed for geometric distortion measurement in MRI including, a 3D phantom recently developed by us.

3.1 2D Phantoms

Among the phantoms developed in 2D, the grid phantom is probably the most popular one. A typical MR image of this phantom is shown in Fig. **1**. This phantom is a two dimensional array of orthogonally interlocking plastic strips immersed in a water solution. It provides a convenient model

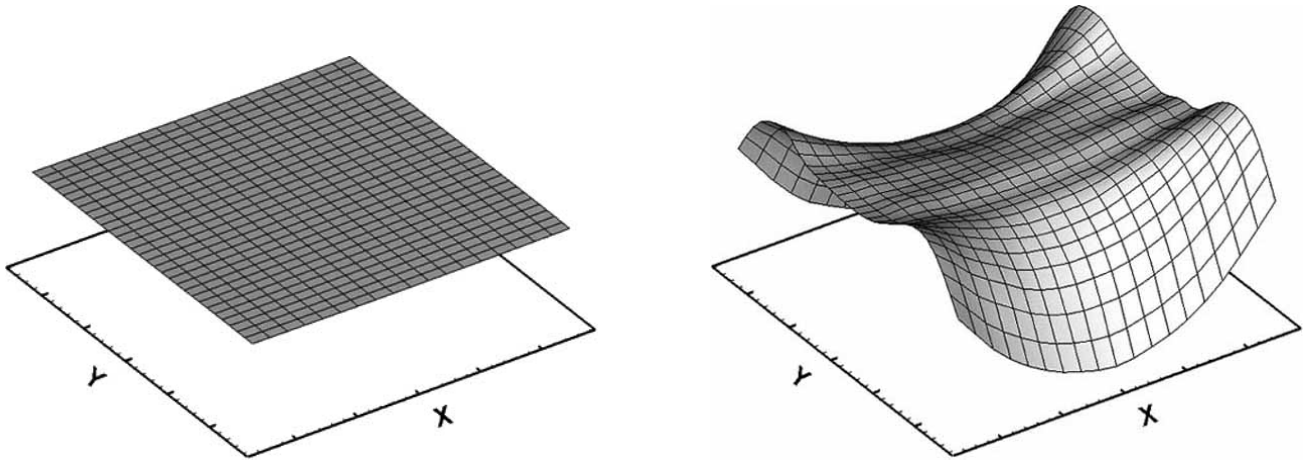

(**2a**) (**2b**)

Fig. (2) . An assumed "flat" slice schematically shown in (a) is actually distorted and may look like the one shown in (b) due to the geometric distortion along the normal of the slice.

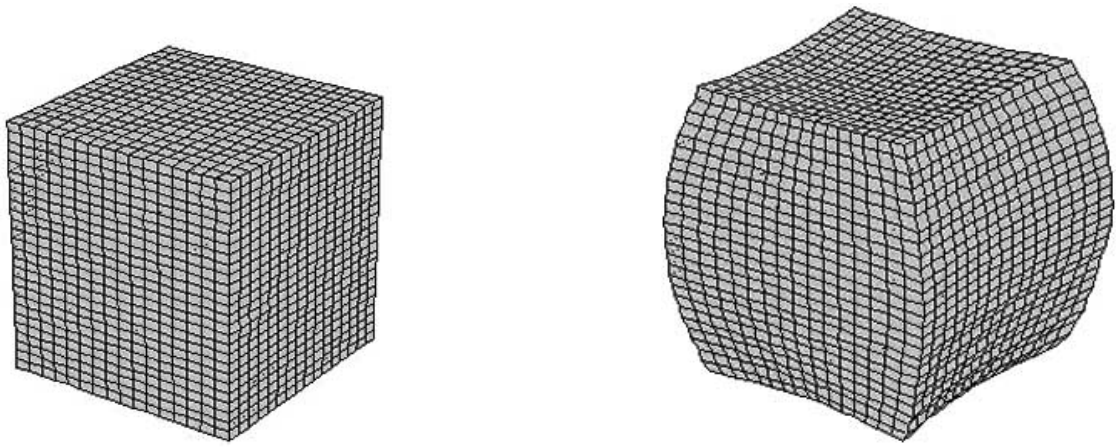

(**3a**) (**3b**)

Fig. (3) A complete measurement of geometric distortion in MRI is demonstrated by using grid points on the surfaces of a cube: their known positions in (a) and their positions in the distorted image space which can be fully "tracked" down in 3D (b).

for displaying geometric distortions in the imaging plane. The other popularly used 2D phantoms employed parallel rods [24, 26], or cylindrical holes filled with water. In a special phantom designed for studying geometric accuracy in spatial localization using a Leksell stereotactic frame, three sets of parallel rods, each aligned along one of the three orthogonal axes, were used [26]. In this way, the geometric distortion can be measured in the three principal planes (coronal, sagittal and axial) in a single set of 3D phantom image.

Although 2D phantoms have the advantage of being easy to use and the geometric distortion in the imaging plane is easily perceptible, they only provide an approximate measurement as noted earlier. If unprimed coordinates (x, y, z) are used to denote the positions of the control points defined by the geometry of the phantom and primed coordinates (x', y', z') for their positions in the distorted image space, the correspondence in a 2D phantom with the control points defined in the xy plane can be described as

$$\begin{pmatrix} x \leftrightarrow x' \\ y \leftrightarrow y' \\ unknown \leftrightarrow z' \end{pmatrix}$$

Because the coordinate of the control points along the normal of the imaging plane (z) is undefined in 2D phantoms, it is unmeasurable (*unknown*).

3.2 3D phantoms

As previously stated, the geometric distortion in MRI is 3D in nature, therefore, its description and measurement needs to be carried out in 3D. In 3D phantoms, the position of the control points is defined along all three orthogonal

directions. The geometric distortion is then completely described by the following correspondence

$$\begin{pmatrix} x \leftrightarrow x' \\ y \leftrightarrow y' \\ z \leftrightarrow z' \end{pmatrix}$$

A number of different designs for introducing control points in 3D into a geometric phantom have been attempted. In one design, spheres of a certain size arranged in three dimensions with the centre of gravity of the spheres defined as the control points have been used [41]. To ensure the accuracy, spheres with a sufficient size were required. This design approach can place a constraint on the number of spheres that can be arranged in a phantom. In another design, parallel rods, very much like those used in the 2D phantoms, were employed, but the rods are tapered [45]. In this way, the linearly varying cross section of the rods along the third direction (the *z* axis) can be used to extract the geometric distortion along the *z* axis through measuring the spot size of the cross section of the rods in the imaging plane. This approach, however, has a weak point. Because the geometric distortion in the imaging plane can significantly alter the spot size of the cross section, the measurement of *z* locations in this way could potentially contain large errors. Very recently, there was another phantom reported in the literature that is principally a 3D design, though the phantom was only demonstrated in 2D [40]. How this phantom can be used in 3D and the accuracy that can be achieved with it still remains to be investigated.

3.3 A New Effective 3D Phantom

Motivated by the lack of an effective phantom that can be conveniently used to provide a comprehensive and complete measurement of the geometric distortion in MRI, a novel 3D phantom has recently been developed [52]. The design of this 3D phantom uses a simple concept that a point in 3D space can be uniquely defined by three orthogonal planes. A photograph of a 3D phantom that was constructed to fit into a body coil based on this design is shown in (Fig. **4**). It has a very simple structure. It consists simply of layers of grid sheets aligned in parallel with equal spacing along the third dimension (the *z* axis) to create a 3D array of points. In this particular phantom, the array contained a total of 10,830 (19x19x30) control points spanning an effective volume of 257.04x259.02x261.0 mm^3 (with intervals of 14.28 *mm*, 14.39 *mm*, and 9.00 *mm*, along the respective *x*, *y* and *z* axes). For more details of this phantom, see Ref. [52].

One of the attractive features in this design approach is that it can easily "incorporate" as many control points as desired in a phantom simply by varying the dimensions of the grid and the width of the grid sheet. Thus, the spatial variation of the geometric distortion can be easily measured with desirable details using a phantom based on this design. The effectiveness of this approach will be demonstrated in the next section where a summary on an extensive study of the geometric distortion in clinical MR systems, carried out recently using this 3D phantom, is presented. Another attractive feature associated with this phantom is accuracy.

Fig. (4). A photograph of a 3D phantom based on a new design approach using a concept that a point in 3D can be defined by the intercepting point of the three orthogonal planes.

The accuracy in a phantom-based technique is largely determined by the accuracy with which the positions of the control points, namely the coordinates *x'*, *y'* and, *z'* in the distorted image space are measured. In some of the previous studies using geometric phantoms, the coordinates of the control points were simply measured through a manual method and in this way the obtainable accuracy is limited by the voxel dimensions. There are a few studies that have employed more sophisticated imaging processing techniques, and the coordinates of the control points were measured with much higher accuracy. Associated with the new 3D phantom, an automated technique based on 3D image processing has been developed [52]. It has been demonstrated that this technique allows the coordinates of the control points in MR phantom images to be extracted with a sub-voxel accuracy. We have recently made further improvements to the accuracy in the measurement of the coordinates of the control points along the *x* and *y* axes.

3.4 Characterization of Geometric Distortion in MRI

There is no standard procedure that has been developed for the characterization of the geometric distortion in MRI. A commonly used method is to measure the distance between a pair of control points selected in an imaging plane and to calculate the deviations from the known distance. This method has been widely used in practice and has also been recommended by AAPM [47] and by the Institute of Physics and Engineering in Medicine (United Kingdom [50]). It is simple, but is basically a 2D method and as noted earlier it can only provide a partial measurement of the geometric distortion. In addition, there is no universally adopted scheme on how the geometric distortion should be characterized and represented. In some recommended methods, geometric distortion is investigated only in the

three imaging planes (coronal, sagittal and axial) which pass through the system's isocentre.

The measurement of the geometric distortion by the new 3D phantom is comprehensive [52]. The geometric distortion within the effective volume of the phantom is fully described by positional deviations along the three orthogonal axes

$$dx(\boldsymbol{r}) = x'(\boldsymbol{r}) - x$$

$$dy(\boldsymbol{r}) = y'(\boldsymbol{r}) - y$$

$$dz(\boldsymbol{r}) = z'(\boldsymbol{r}) - z$$

or

$$d\boldsymbol{r}(\boldsymbol{r}) = \boldsymbol{r}'(\boldsymbol{r}) - \boldsymbol{r}$$

These positional deviations can be obtained, for example, using an interpolation method from the measured positional deviations at the control points

$$dx_{i,j,k} = x_{i,j,k} - x_{i,j,k}$$

$$dy_{i,j,k} = y_{i,j,k} - y_{i,j,k}$$

$$dz_{i,j,k} = z_{i,j,k} - z_{i,j,k}$$

or

$$d\boldsymbol{r}_{i,j,k} = \boldsymbol{r}_{i,j,k} - \boldsymbol{r}_{i,j,k}$$

In this way, a comprehensive characterization scheme can be developed and such a scheme has been proposed in Ref. [53]. There are a number of attractive features in this new scheme. Firstly, the use of the positional deviations allows a unique definition of the distortion by comparing a point's true position with its displaced position measured in the distorted image space. This measure of geometric distortion is particularly useful for MR image-based spatial localization. Secondly, the parameterized data in the scheme are always given with respect to a well-defined volume of interest. In the scheme discussed in [53], there are two types of volume of interest: a rectangular parallelepiped (including cube), and a sphere, which have been considered. Clearly, these two volumes of interest are relevant to body and neuro imaging applications. The rectangular parallelepiped has its surfaces parallel to the standard imaging planes. Both VOIs have their centre chosen at the isocentre. The key parameters used in this scheme include the maximum absolute positional deviations along the *x*, *y* and *z* axes ($|dx|_{max}$,$|dy|_{max}$ and $|dz|_{max}$) and the maximum absolute deviation in positional vector ($dr_{max} \equiv \| d\boldsymbol{r} \|_{max}$) within a given volume of interest. These maximum positional deviations are determined through a re-sampling process. By using a re-sampling process, the surfaces of VOI are well represented, allowing the true maxima to be found within a given volume of interest.

4. GEOMETRIC DISTORTION IN REPRESENTATIVE MRI SYSTEMS

In this section, the geometric distortion due to the inhomogeneity of the static field and the nonlinearity of the gradient fields in some representative MRI systems is reviewed.

4.1 MR Systems with Superconducting Magnets

In clinical MRI systems equipped with superconducting magnets, geometric distortion due to the gradient field nonlinearity is usually much larger than that arising from the static field inhomogeneity. This is especially the case in the new generation of MRI systems in which shorter gradient coils are used for achieving stronger gradient performance. For example, in a Siemens Sonata 1.5 T system, the geometric distortion arising from the static field inhomogeneity can be reduced within a fraction of one millimeter using advanced shimming technologies within a volume of 240^3 mm^3. In comparison, the geometric distortion caused by the gradient field nonlinearity can be as large as 10 *mm*. As a result, correction for geometric distortion due to the gradient field nonlinearity has become necessary. In order to minimize the geometric distortion from gradient field nonlinearity in MR images, major MRI vendors such as GE and Siemens have now implemented a correction procedure before the frequency domain data (the MR image) are finally generated.

Geometric distortion has been reported on a large number of MRI superconducting systems [21-36, 42]. However, most of these studies were made using 2D phantoms providing only a partial measurement of the geometric distortion. In addition, different studies used slightly different methods for assessing the geometric distortion. The volume of interest or region of interest (if in 2D) used in these studies also varied. Besides, the systems investigated in some earlier studies might have had significant upgrading to the system and the measured data may have now become irrelevant. Therefore, no attempt was made to recollect all these data in this mini-review. Instead, the geometric distortion data presented below were largely drawn from a recent study on four clinical MR systems (two from GE and two from Siemens) using our 3D phantom [54]. This study is probably the most comprehensive study ever carried out on hardware-related geometric distortion in MRI to date.

The geometric distortion in a GE TwinSpeed 1.5 T system may be a good representation of the geometric distortion in contemporary MRI systems with superconducting magnets. In this system, as the name suggests, there are two sets of gradient coils. The gradient set named Zoom mode is a representative set of faster and stronger gradients which normally have greater nonlinearity problems. The geometric distortion in the Zoom mode measured as the maximum absolute positional deviations in the axial planes at various *z* positions is presented in Fig. **5**. As shown, the maximum absolute positional deviations in the central slices ($|z| < 75$ *mm*) are relatively small (< 3 *mm*) but they increase rapidly as they move away from the central region ($|z| > \sim 75$ *mm*). It should be pointed out that the geometric distortion (except along the *z* axis) presented here does not represent the full effect of the gradient field nonlinearity because the vendor's correction (applied in the *xy* plane) was used in the acquisition of the phantom MR images. The geometric distortions were much greater when the full effect of the gradient field nonlinearity was investigated [54]. The other gradient set denoted as Whole mode in this system represents gradient coils with much better linearity and slower slew rate. The mapped geometric distortion for the Whole mode is summarized in Fig. **6**. The maximum positional deviations in this gradient set are generally small between 1 and ~4 mm in the entire VOI (240^3 mm^3). Similar geometric distortion patterns have also been observed for the two Siemens representative systems, a

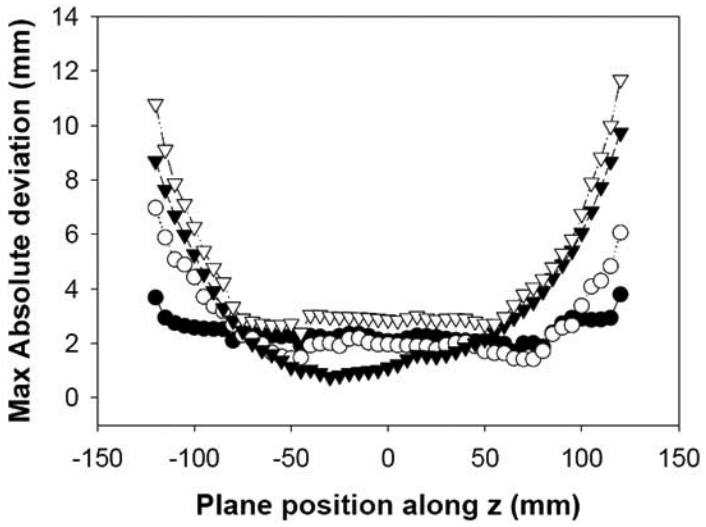

Fig. (5). The maximum absolute positional deviations (●: | *dx* |$_{max}$, o: | *dy* |$_{max}$, ▼: | *dz* |$_{max}$, : dr_{max}) of the geometric distortion measured in a GE TwinSpeed 1.5 T MRI system (Zoom mode) with vendor's correction applied in the *xy* plane.

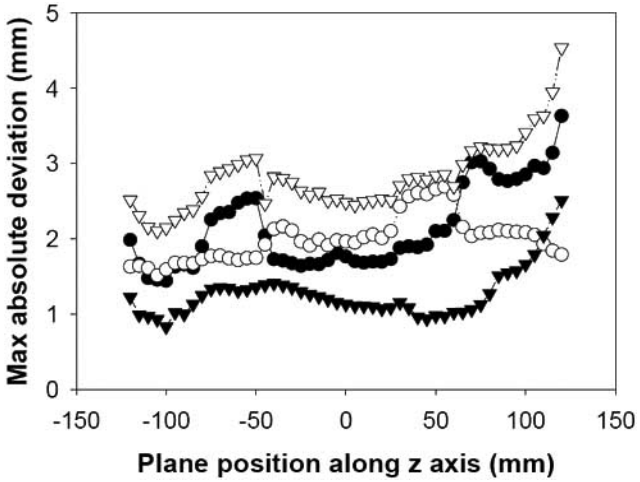

Fig. (6). The maximum absolute positional deviations (●: | *dx* |$_{max}$, o: | *dy* |$_{max}$, ▼: | *dz* |$_{max}$, : dr_{max}) of the geometric distortion measured in a GE TwinSpeed 1.5 T MRI system (Whole mode) with vendor's correction applied in the *xy* plane.

Sonata and a Quantum [54]. As expected, the geometric distortion in the Sonata which had a fast-speed gradient set was much larger than that in the Quantum which was equipped with a gradient system of the previous generation. For a complete description of the geometric distortions in these systems, see Ref. [54].

For neuro-imaging applications, the geometric distortions in these systems were also investigated within a spherical VOI (r = 95 *mm*). As expected, the geometric distortion was much less in this spherical VOI. If measured by the maximum absolute positional deviations, the maximum geometric errors were in the range of 2.0 to 2.5 *mm* in all these systems [54]. A typical result for the maximum positional deviations measured on the surface of spheres with different radii is shown in Fig. **7**. In this particular system, the maximum absolute positional deviations along the *y* and *z* axes were 1.5 *mm* or less and that along the *x* axis was about ~2.0 *mm* or less.

4.2 MR Systems with Resistive or Permanent Magnets

Low field MR systems currently employed in clinical service mainly include those operating at ~0.2 T using a permanent or resistive magnet. Below, the geometric distortion in three representative low field systems, recently reported in the literature, is summarized. These systems have been reported in routine use for radiation therapy simulations.

A geometric distortion study on a low field 0.2*T* MR system (MRP 20 EX; Hitachi Med. Co. Tokyo) has been carried out using a 2D grid phantom with an effective area of 240x240 mm^2 [38]. The authors reported that within 120 *mm* of the image centre (the isocentre), the maximum positional

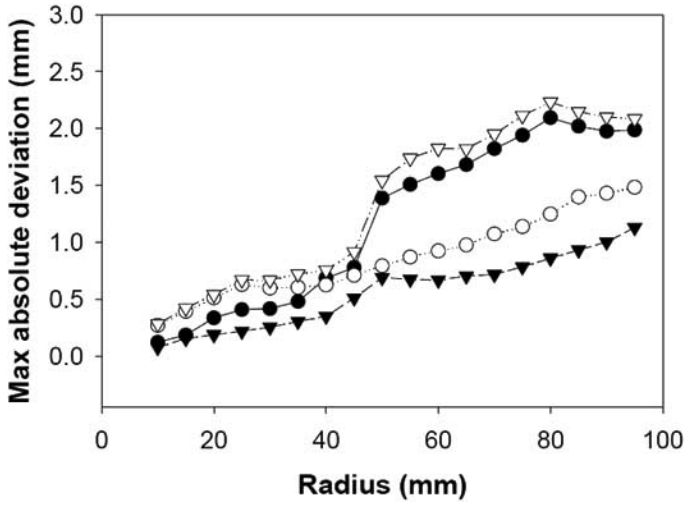

Fig. (7). The maximum absolute positional deviations (●: | dx |$_{max}$, o: | dy |$_{max}$, ▼: | dz |$_{max}$, : dr_{max}) of the geometric distortion measured in a GE TwinSpeed 1.5 T MRI system (Zoom mode) with vendor's correction applied in the *xy* plane on surface of spheres of different radii.

deviations were between 3.5 and 5.0 *mm* but in the majority of the area, the positional deviations were less than 2 *mm*. Larger geometric distortions were observed with the maximum positional deviations of 12.6 *mm* to 15.0 *mm* in a larger field of view. They also investigated the geometric distortion by using different imaging sequences and observed up to ~15% differences in the measured maximum positional deviations. The geometric distortion in a 0.23*T* open MRI system (Philips Medical Systems, Cleveland, OH 44143) has been comprehensively studied recently [39]. The geometric distortion was investigated with and without vendor's correction using a 2D grid phantom. Without correction, distortions exceeding 20 *mm* were observed at the image periphery. The geometric distortion was significantly reduced after vendor's correction. Within the spherical VOI of r = 100 *mm*, the positional deviations were reduced to below 2 *mm* and were less than 5 *mm* within a larger spherical VOI (r = 20 cm). In a more recent study on a 0.2 *T* MRI system (Siemens Magnetom Open viva), maximum positional deviations of 28.0 *mm* and 16.0 *mm* along the x and y axes in the axial plane were reported [40]. These authors also studied the effectiveness of two correction methods, one provided by the vendor and one developed by the authors. After using the vendor's correction, the maximum positional deviations were reduced from 28.0 *mm* and 16.0 *mm* to 20.9 *mm* and 11.1 *mm*, respectively. The in-house correction method gave a better performance with the maximum positional deviations reduced to 13.7 *mm* and 7.5 *mm*, respectively.

It should be pointed out that in all these studies, the geometric distortions were measured using 2D phantoms. In addition, there were few details given on how the positions of the control points were measured. Presumably, they were all measured manually. Thus, the accuracy in these measurements is limited by the pixel's dimensions. The pixel's dimensions in the imaging plane used in these studies varied between 1.25 *mm* and 1.76 *mm*.

5. METHODS FOR CORRECTING GEOMETRIC DISTORTION

Correction for geometric distortion in MR images is often carried out as a post-processing step. Clearly, a full correction needs to be carried out in 3D which obviously can only apply to volumetric image data. For single slice or non-contiguous slices (slices acquired with gaps in between), the correction can only be done approximately within the slice plane. The correction methods currently supplied by the major MR vendors such as GE and Siemens work only in 2D as mentioned in the previous section (the 3D versions of these methods may become available soon).

For a full correction in 3D, the correction problem is to find the functions that relate the coordinates in the distorted image space (x', y', z') and in the undistorted physical space (x, y, z)

$$x' = f_x(x,y,z)$$
$$y' = f_y(x,y,z)$$
$$z' = f_z(x,y,z)$$

For easy reference $f_x(x,y,z)$, $f_y(x,y,z)$ and $f_z(x,y,z)$ are referred to as mapping functions. When these mapping functions are obtained, the correction simply involves a re-sampling of the image volume. The re-sampling is usually done using an interpolation method. There are a large number of interpolation methods that can be used for re-sampling. The ones that are most popularly used are the tri-linear interpolation and sinc interpolation. The tri-linear interpolation is extremely efficient while the sinc interpolation usually offers better quality but at a considerably high computational cost.

There have been a number of different correction methods developed to obtain the mapping functions, $f_x(x,y,z)$, $f_y(x,y,z)$ and $f_z(x,y,z)$ for correcting geometric distortion caused by MR hardware. For example, to correct geometric distortions caused by the gradient field nonlinearity the use

of spherical harmonics expansion for modeling the mapping functions was proposed [55]. These functions can be calculated from the known geometry of the gradient coils [56, 57] or derived numerically through the mapped fields by a magnetic field camera (MetroLab Instruments SA, Geneva, Switzerland; http://www.metrolab.ch). In phantom-based methods, the use of polynomials to model the mapping functions seems to be a popular choice. Polynomials of various orders have been used in modeling geometric distortion in MRI [41,43,57].

Spherical harmonics functions or polynomial functions are global functions and they are analytically compact and contain only a small number of parameters. However, there are some disadvantages associated with the use of global functions for modeling geometric distortions in MRI. Firstly, there is a problem with the optimal selection of the terms to be used in a given modeling problem. Inclusion of high-order terms may provide a better "fit" to the source data, but they do not necessarily offer the best modeling solution. Secondly, there are problems with the optimal selection of the origin and the axes. For example, using the symmetry of the gradient fields as predicted theoretically in the modeling process clearly neglects any possible misalignment of the gradient coils either due to a less perfect workmanship or during use. Thirdly, global functions can sometimes lack the "spatial flexibility" required to model local features satisfactorily.

The densely sampled geometric distortion data using our new 3D phantom can allow the use of local piecewise interpolation to obtain the mapping functions. Therefore, correction of the geometric distortion in conjunction with this phantom can be carried out using a range of piecewise interpolation methods. In fact, because of the high density of the source data obtained with this phantom, we used the tri-linear interpolation, an efficient interpolation method in 3D, in the correction of the geometric distortions measured in clinical MR systems. The results were extremely satisfactory [58]. A representative example of the residual geometric distortion measured in the corrected MR phantom images in a clinical MRI system is shown in Fig. **8**. Here, the maximum absolute positional deviations are all within 1 *mm* with most falling within a fraction of 1 *mm*. A distinctive feature of using local interpolation methods in conjunction with the geometric distortion data measured with our new phantom is that it works uniformly well in the entire effective volume of the phantom as indicated in Fig. **8**. This is in strong contrast to the correction results obtained with the vendors' correction methods (see Fig. **5**, for example, where the correction became progressively less effective in more remote slices at $|z| \geq \sim 75$ *mm*). Our correction also performed equally well on significantly larger geometric distortions due to the full effect of the gradient field nonlinearity (using MR images acquired with vendor's correction off). For interested readers, see Ref. [58].

It is apparent that in conjunction with our 3D phantom, other more sophisticated piecewise interpolation methods can also be used. Well-known piecewise interpolation methods include the thin-plate spline and multi-quadratic method [59, 60]. Both these methods can provide highly desirable smoothness and continuity with extremely high flexibility. Originally, these models were developed in 2D. In principle, they can be extended to 3D but will significantly increase the computational time. In order to keep the computational time low, a hybrid algorithm has been developed combining a 2D interpolation in the *xy* plane using either the thin-plate spline or the multi-quadratic method, and a one-dimensional interpolation method, the cubic spline interpolation, along the *z* axis. However, no additional improvement was found in using this hybrid interpolation compared with using the tri-linear interpolation. This is another strong indication of the effectiveness and the accuracy demonstrated by our phantom-based technique.

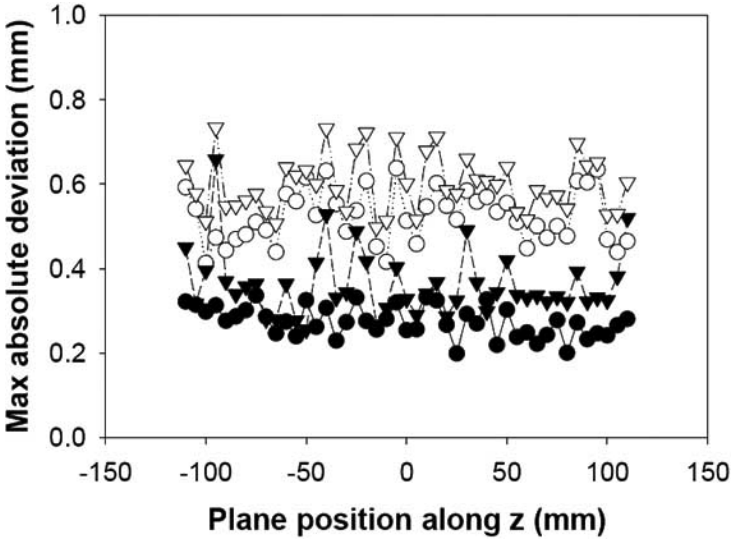

Fig. (8). The maximum absolute positional deviations (●: | dx |$_{max}$:, o: | dy |$_{max}$, ▼: | dz |$_{max}$, : dr_{max}) of the residual geometric distortion measured after correction using a new 3D phantom-based technique in a Siemens Quantum 1.5 T system.

6. DISCUSSION

In contemporary clinical MR systems the nonlinearity of the gradient fields is usually the major source of the geometric distortion in structural MR images. With advanced shimming technologies, the geometric distortion associated with the inhomogeneity of the static field is small compared with that arising from the gradient field nonlinearity. This is particularly so in the new generation of MR systems equipped with shorter gradient coils. As MRI technologies are constantly being advanced, high demand for faster and stronger gradients has led to the use of shorter gradient coils with a compromise in gradient field linearity. As a consequence, the reduced linearity in the gradient fields generated by these shorter gradient coils has led to an increase in the related geometric distortion.

It has now become a standard and accepted procedure as a part of the image-generating process to include correction for geometric distortion caused by gradient field nonlinearity. Major vendors such as GE and Siemens all have correction algorithms implemented in their MR systems. These correction algorithms have significantly reduced the geometric distortion caused by the gradient field non-linearity. A complete analysis on vendors' correction algorithms in some representative clinical MR systems can be found in Ref. [54]. However, there are some limitations to these correction algorithms that are worthy of discussion.

Firstly, these correction algorithms only work in 2D in the current version. As strongly emphasized in this mini-review, geometric distortion in MRI is 3D in nature and complete correction requires a 3D approach. This is particularly important in MR volumetric imaging for applications in spatial localization and volumetric studies. If we take the GE TwinSpeed Zoom mode as a specific example, we can show that (in Fig. **5**) significantly large geometric distortions along the *z* axis are still present although the vendor's correction has significantly reduced the geometric distortion along the *x* and *y* axes (the "original" geometric distortion along the *x* and *y* axes was much greater [54]). Therefore, the MR images could still contain large overall geometric errors (represented by *dr* in Fig. **5**). Obviously, this can cause detrimental effects if the "partially" corrected MR images were to be used, for example, for spatial localization in radio-surgery or in MR image-based biopsy. Secondly, the vendor's correction algorithms do appear to have a limitation on the amount of geometric distortion that can be corrected. If measured by the residual geometric distortions after correction, the distortions were still relatively large. In the systems investigated by us recently, the maximum absolute positional deviations within a volume of 240^3 mm^3 were still in the range of ~2.0 *mm* to 7.0 *mm* [54]. The effectiveness of the vendor's correction also varied considerably and it became much less effective in slices further away from the system's isocentre, especially for correcting large geometric distortions arising from the gradient systems of the new generation such as the GE TRM Zoom and Siemens Sonata.

It is difficult to speculate on the possible reasons for the limitations shown by the vendor's correction algorithms because the details of the algorithms were unknown to us. However, it is possible to suggest that these correction algorithms may be based on a set of parameterized data that were measured at the time the gradient coils were constructed. If this is the case, it is obvious that any temporal changes in the gradient field nonlinearity during use cannot properly be taken into account in the correction. It is also likely that global mapping functions rather than piecewise interpolations were used in the correction. This may give an explanation why the correction algorithms performed less effectively in outer areas [54].

The 3D phantom-based technique for measurement and correction of geometric distortion recently developed by us should overcome some of these shortcomings. Noticeably, the two most attractive features of this technique are its effectiveness and accuracy. As stated in section 3.3, the novel design approach easily allows a dense array of control points to be introduced within a given volume of interest (limited only, in principle, by structural stability required in the construction). Thus, the spatial variation of the geometric distortion can be measured with sufficient details. Another significant benefit is that piecewise interpolation can be used in correction. The accuracy of this method has been demonstrated to be extremely high [52]. For example, using the maximum absolute positional deviations measured in the corrected phantom images as an indication, they were all below 0.8 *mm* with an average value of ~0.5 *mm* for the four MRI systems investigated in a recent study [58]. The exceptionally high performance demonstrated in the range of geometric distortions present in these MR systems is a strong indication of the successful use of the flexible piecewise interpolation in the correction. Additionally, the measurement using our 3D phantom is extremely simple. The required single 3D phantom scan only takes about 10 to 30 minutes (depending on the sequence used and the averages required) and it can be acquired unattended. When the phantom MR image is acquired, the fully automated algorithm that extracts the positions of the control points takes a few minutes. Thus, this new technique can make routine measurement at any desirable interval easily possible.

Geometric distortion due to susceptibility difference has not been discussed in this review. Briefly, this type of geometric distortion can also be present in structural MRI. Taking human brain as a specific example, large geometric distortions due to the susceptibility difference can occur at tissue/air boundaries. The difference in the relative permeability values of air and tissue is approximately 9 *ppm* which can result in significantly large geometric distortions up to a few voxels in certain regions such as sinuses. It should be noted that the geometric distortion due to susceptibility difference is manifested similarly to that caused by the static field inhomogeneity. For example, the magnitude of the distortion is also dependent on the gradient strength used. It can be suppressed by using stronger gradients. Geometric distortion due to the susceptibility difference is obviously field-dependent and it increases at high magnetic fields. In fact, the susceptibility difference caused geometric distortion has now become a major issue for MR imaging at 3T or above.

In summary, geometric accuracy in MRI is still an issue in magnetic resonance imaging today. The hardware-related

geometric distortion in contemporary MR systems has been reviewed in this paper, especially in relation to structural MRI. High level of geometric distortion can still be present in today's MR systems. Although not normally an issue in clinical examinations, geometric distortion in MRI is a major concern in applications where high precision is required. To reduce geometric distortion due to MR hardware to within a fraction of one millimeter in structural MR images is still some distance away. This level of accuracy may be required in certain applications such as spatial localization in radiation treatment and MR image-based volumetric measurement. For example, in the case of spatial localization in treating brain tumors, geometric accuracy of better than 1 *mm* is often regarded as the minimum requirement. For MR volumetric imaging, we have seen structural MRI play an increasingly important role in the study of brain diseases in recent years. A representative example is the use of structural MRI in the study of Alzheimer's disease, which has resulted in a large volume of MRI literature in this very important research area. Many quantitative studies on brain atrophy and its progression rate have been reported. However, there have been some concerns on the quality of the published data. One major concern is in respect of image quality control. To date, there appears to have been little effort devoted to this issue. A general problem in any image-based quantification like using MRI is the difficulty in estimating the uncertainties (or the errors) associated with the extracted volumes or areas. This is an extremely challenging problem. It has begun to receive some attention recently. Clearly, to have an effective method which can measure and correct the geometric distortion associated with structural MR images with sub-millimeter accuracy is an important step in successfully addressing this problem.

ACKNOWLEDGEMENTS

Deming Wang would like to thank Christine Chester–Jones whose help has made significant improvement in the presentation of the manuscript, and Liu Feng for help with the preparation of some of the figures.

REFERENCES

[1] Takacs I, Hamilton AJ. Techniques in Neurosurgery 2003; 8: 11-26.
[2] Mandybur GT. Techniques in Neurosurgery 2003; 8: 6-10.
[3] Yu C, Petrovich Z, Apuzzo ML, Luxton G. J Appl Clin Med Phys 2001; 2(1): 42-50.
[4] Major T, Petranyi A, Varjas G, Nemeth G. Magy Onkol 2002; 46(3): 239-45.
[5] Fransson A, Andreo P, Potter R. Strahlenther Onkol 2001; 177(2): 59-73.
[6] Burchiel KL, Nguyen TT, Coombs BD, Szumoski J. Stereotact Funct Neurosurg 1996; 66(1-3): 123-36.
[7] Derosier C, Delegue G, Munier T, Pharaboz C, Cosnard G. J Radiol 1991; 72(6-7): 349-53.
[8] Alexander E 3rd, Kooy HM, van Herk M, Schwartz M, Barnes PD, Tarbell N, Mulkern RV, Holupka EJ, Loeffler JS. J Neurosurg 1995; 83(2): 271-6.
[9] Phillips MH, Kessler M, Chuang FY, *et al.* Int J Radiat Oncol Biol Phys 1991; 20: 881-889.
[10] Kondziolka D, Dempsey K, Lunsford LD, *et al.* Neurosurgery 1992; 30: 402-7.
[11] Jessard P, Balaban RS. Magn Reson Med 1995; 34: 65-73.
[12] Reber PJ, Wong EC, Buxton RB, Frank LR. Magn Reson Med 1998; 39(2): 328-30.
[13] Hutton C, Bork A, Josephs O, Deichmann R, Ashburner J, Turner R. Neuroimage 2002; 16(1): 217-40.
[14] Burkhardt S, Schweikard A, Burgkart R. Med Imag Anal 2003; 7(3): 221-36.
[15] Schenck JP. Med Phys 1996; 23: 815-43.
[16] Li S, Williams GD, Frisk TA, Arnold BW, Smith MB. Magn Reson Med 1995; 34(2): 268-75.
[17] Collins CM, Yang B, Yang QX, Smith MB. Magn Reson Imag 2002; 20: 413-424.
[18] Yoder DA, Zgao Y, Paschal CB, Fitzpatrik JM. Magn Reson Imag 2004; 22: 315-328.
[19] Ludeke KM, Roschmann P, Tischler R, Magn Reson Imag 1985; 3: 329-43.
[20] Bhagwandien R, Moerland MA, Bakker CJG, Beersma R, Lagenijk JJW. Magn Reson Imag 1994; 12: 101-7.
[21] Piovan E, Zampieri PG, Alessandrini F, *et al*. Stereotact Funct Neurosurg 1995; 64: 228-232.
[22] Moreland M, Beesma R, Bhagwandient R, Wijrdeman HK, Bakker C. Phys Med Biol 1995; 40: 1651-64.
[23] Prott FJ, Haverkamp U, Willich N, Resch A, Stober U, Potter R. Radiother Oncol 1995; 37: 221-4.
[24] Walton L, Hampshire A, Forster DMC, Kemeny AA. Neurosurgery 1996; 38: 170-178.
[25] Walton L, Hampshire A, Forster DMC, Kemeny AA. Neurosurgery 1997; 41: 131-139.
[26] Yu C, Apuzzo MLJ, Zee CS, Petrovich Z. Neurosurgery 2001; 48: 1092-1099.
[27] Sumanaweera TS, Glover G, Song S, Adler JR, Napel S. Magn Reson Med 1994; 31: 40-47.
[28] Sumanaweera TS, Adler JR, Napel S, Glover GH. Neurosurgery 1994; 35: 696-704.
[29] Ramani R, Ketko MG, O'Brien PF, Schwartz ML. Med Phys 1995; 22: 1343-46.
[30] Orth RC, Sinha P, Madsen EL, *et al*. Neurosurgery 1999; 45: 1423-1431.
[31] Bednarz G, Downes MB, Corn BW, Curran WJ, Goldman HW. Neurosurgery 1999; 45(5): 1156-61.
[32] Maciunas RJ, Fitzpatrick JM, Gadamsetty S, Maurer CR Jr. Stereotact Funct Neurosurg 1996; 66(1-3): 137-40.
[33] Schad L, Lott S, Schmitt F, Sturm V, Lorenz WJ. J Compu Assist Tomogr 1987; 11: 499-505.
[34] McRobbie DW. Med Phys 1997; 24: 737-42.
[35] Dubois DF, Bice Jr WS, Prestige BR. Med Phys 2001; 28: 2280-84.
[36] Michiels J, Bosmans H, Pelgrims P, Vandermeulen D, Gybels J, Marchal G, Suetens P. Magn Reson Imag 1994; 12: 749-65.
[37] Mizowaki T, Nagata Y, Okajima K, *et al*. Radiology 1996; 199(3): 855-60.
[38] Mizowaki T, Nagata Y, Okajima K, Kokubo M, Negoro Y, Araki N, Hiraoka M. Radiother Oncol 2000; 57: 237-242.
[39] Mah D, Stechner M, Palacio E, *et al.* Med Phys 2002; 29: 2541-2547.
[40] Petersch B, Bogner J, Fransson A, Lorang T, Potter R. Radiother Oncol 2004; 71: 55-64.
[41] Breeuwer M, Holden M, Zylka W. Proc SPIE 2001; 4322: 1110-1120.
[42] Holden M, Breeuwer M, Mcleish K, Hawkes DJ, Keevil SF, Hill DLG. Proc SPIE 2001; 4322: 69-78.
[43] Kawanaka A, Takagi M. J Phys E. Sci Instrum 1986; 19: 871-875.
[44] Chang H, Fitzpatrik JM. IEEE Trans Med Imaging 1992; 11(3): 319-29.
[45] Schneider E, Linz AM, Repinski GA. 1996; U S patent 5; 545, 995.
[46] Bammer R, Markl M, Barnett A, Acer B, Alley MT, Pelc NJ, Glover GH, Moseley ME. Magn Reson Med 2003; 50: 560-69.
[47] Price RR, Axel L, Morgan T, *et al*. Med Phys 1990; 17(2): 287-295.
[48] Lerski RA, de Certaines JD. Magn Reson Imag 1993; 11(6): 817-33.
[49] Lerski RA. Magn Reson Imag 1993; 11(6): 835-9.
[50] Lerski RA, de Wilde J, Boyce D, Ridgeway J. IPEM Report 80. York: The Institute of Physics and Engineering in Medicine 1998.
[51] NEMA, Document MS 2-2003 (National Electrical Manufacturers Association, Washington, DC, 2003).
[52] Wang DM, Doddrell DM, Cowin G. Magn Reson Imag 2004; 22: 529-42.
[53] Wang DM, Doddrell DM. Med Phys 2004; 31: 2212-18.
[54] Wang DM, Strugnell W, Cowin G, Doddrell DM, Slaughter R. Magn Reson Imag 2004; (Nov. issue).
[55] Glover GH, Pelc NJ. 1986; U S patent 4, 591, 789.
[56] Liu H. MAGMA 2000; 10(2): 75-9.

[57] Langlois S, Desvignes M, Constans JM, Revenu M. J Magn Reson Imag 1999; 9: 821-831.
[58] Wang DM, Strugnell W, Cowin G, Doddrell DM, Slaughter R. Magn Reson Imag 2004; (Nov. issue).
[59] Franke R. Mathematics of Computation, 1982; 38: 181-200.
[60] Hardy RL. J Geophys Res 1975; 10: 321-332.

Received: October 25, 2004 Accepted: November 01, 2004